Long silence on the East Anatolian Fault Zone (Southern Turkey) ends with devastating double earthquakes (6 February 2023) over a seismic gap: implications for the seismic potential in the Eastern Mediterranean region

Hayrullah Karabulut, Sezim Ezgi Güvercin, James Hollingsworth, Ali Özgün Konca

Long silence on the East Anatolian Fault Zone (Southern Turkey) ends with devastating double earthquakes (6 February 2023) over a seismic gap: Implications for the seismic potential in the Eastern Mediterranean region

Karabulut H., Güvercin S.E., Hollingsworth, J., Konca A.Ö.

Accepted Manuscript

Karabulut, H.; Güvercin, S. E.; Hollingsworth, J.; Konca, A. Ö. (2023): Long silence on the East Anatolian Fault Zone (Southern Turkey) ends with devastating double earthquakes (6 February 2023) over a seismic gap: implications for the seismic potential in the Eastern Mediterranean region. Geological Society of London. Collection.

https://doi.org/10.6084/m9.figshare.c.6567094.v2

Abstract

On the 06th February 2023, an earthquake with magnitude ~Mw7.0 on the Narlı Fault, a fault subparallel to the East Anatolian Fault Zone (EAFZ), initiated a chain of large earthquakes on the EAFZ. The earthquakes occurred in a seismic gap with low geodetic strain rates, low background seismicity, where deformation is distributed across a wide fault zone and long recurrence time of historical earthquakes. The ~50 km long rupture of the Narlı Fault towards Pazarcık, led to Mw7.8 left-lateral strike-slip earthquake breaking ~300 km section of the ~600 km long EAFZ bilaterally with a total duration of more than 80 s. Toward the southwest, the rupture propagated on ~100 km long Amanos segment with a peak surface offset of 5 m, before diminishing toward the Hatay graben. In the northeast direction, the rupture reached a peak surface offset of 7 m before sharply declining at the termination of the 2020, Mw6.8 Sivrice earthquake rupture. A second large earthquake with Mw7.6 occurred 9 hours later on the Çardak Fault, located at the western margin of (and sub-parallel to) the EAFZ breaking the surface with almost 9 m left-lateral slip (average of ~4 m). Following these large earthquakes, the increase in the regional stress led to a rapid seismic activation in a broad region from central to eastern Anatolia loading the faults at various scales and increasing seismic hazard. Two weeks after the initiation of the seismic crisis, a third earthquake with Mw6.4 occurred at the southern boundary of the Hatay graben, near the southwestern termination of the Amanos rupture. The earthquakes caused significant loss of human life, devastating 12 cities. We evaluate the observations prior to the ruptures, present preliminary seismological results with surface displacements from sub-pixel correlation of optical satellite images and the stress perturbations computed on the nearby faults based on preliminary slip models. The reevaluation of the seismic potential in light of the recent and historical earthquakes provides some new insight on seismic hazard assessment. The recent series of events on the EAFZ is an important reminder that large faults can generate very large earthquakes of multiple segments. The seismic potential of large earthquakes on these fault zones can only be estimated by considering multiple seismic cycles, and moment deficits from very large earthquakes.

Introduction and Regional Settings

The East Anatolian Fault Zone (EAFZ) is bounded by the Karlıova Basin to the northeast, where the relative motion between Eurasia and Arabia is distributed across the North Anatolian Fault (NAF), EAFZ and the Varto Fault Zone (VFZ) (Arpat and Şaroğlu, 1972, Şengör, 1979; Şaroğlu, 1985) (Figure 1). In the southwest, the EAFZ joins the Dead Sea Fault (DSF) at Kahramanmaraş Triple Junction (KMTJ), near Türkoğlu (e.g. Jackson and McKenzie, 1984; Hempton, 1987; Muehlberger and Gordon, 1987; Barka and Kadinsky-Cade, 1988) and continues towards Cyprus Arc where the convergence is accommodated between the Nubia and Anatolia plates (McKenzie, 1972; Dewey et al., 1973) (Figure 1). Geologic and geomorphological studies on the EAFZ indicate that the slip rate systematically decreases from ~10 mm/yr near Karlıova to ~4 mm/yr near Türkoğlu (Mahmoud et al., 2013; Koç and Kaymakçı, 2013; Bayrak et al., 2015; Aktuğ et al., 2016). Further southwest, the slip rate decreases further down to ~2.5 mm/yr on the main fault and to ~1 mm/yr on sub-parallel faults (Herece, 2008; Duman and Emre, 2013; Gülerce et al., 2017; Yönlü et al., 2017).

As a consequence of the geometry and the plate motion direction as well as significant slip rate variations, the EAFZ holds significant geometric complexities over its ~600 km length displaying seismicity patterns with gaps, localized clusters and sections of diffuse activity (Güvercin et al., 2022 and references therein). The geometric complexities along the fault are frequently used as a basis for fault segmentation associated with the rupture extents of the historical earthquakes (Duman and Emre, 2013).

From northeast to southwest, the various segments experienced moderate size earthquakes since 2010; The Kovancılar earthquake in 2010 broke ~30 km of the northeasternmost extent of the EAFZ (Tan et al., 2011). The adjacent Palu segment (~80 km long) partially ruptured between 2010-2011 with two moderate earthquakes (Mw5.4 and Mw6.1) and has been continuously active

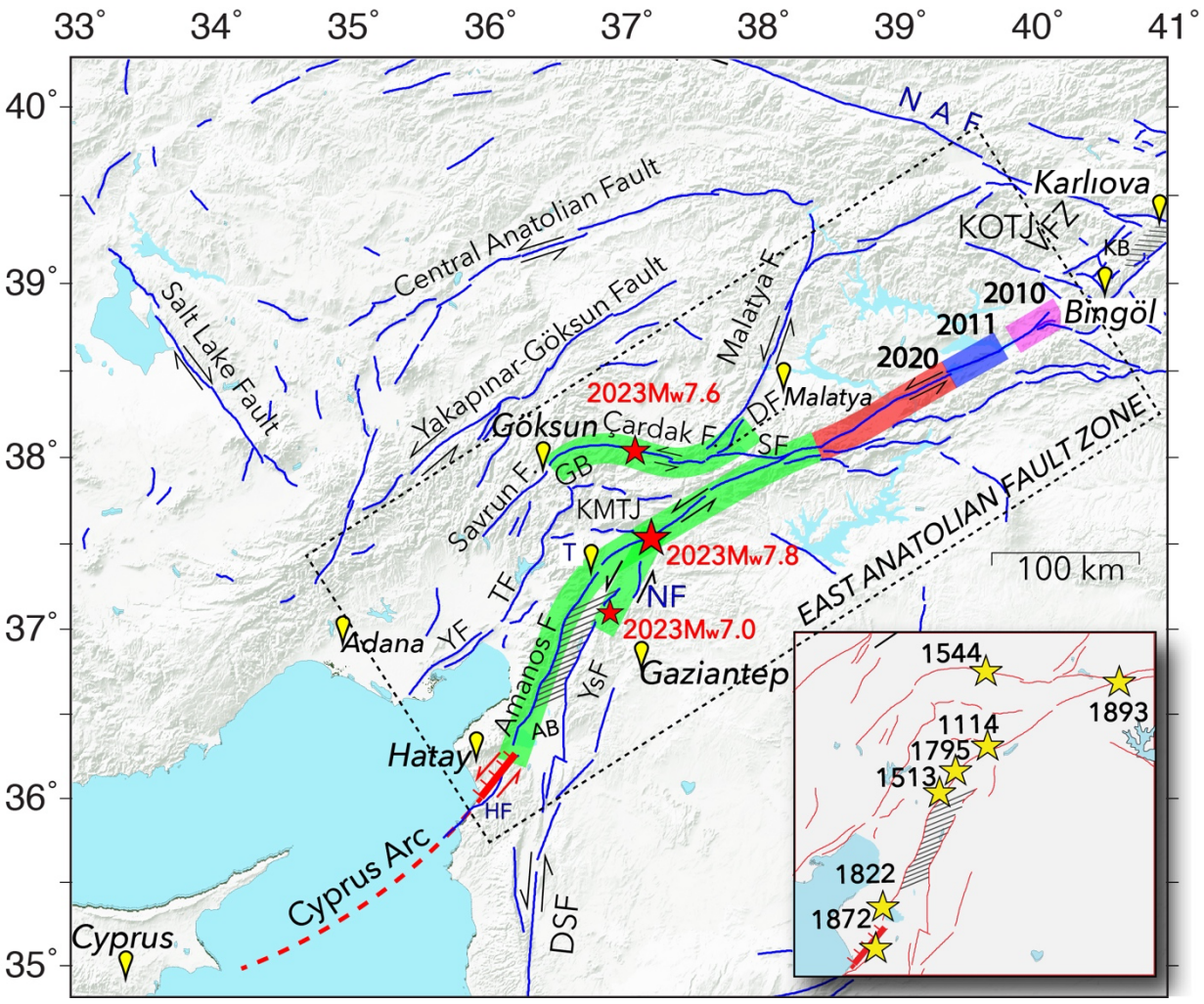

Figure 1: Tectonic setting of the study region with shaded topography (http://dds.cr.usgs.gov/srtm/version2 1/SRTM30/). Faults are shown by thin blue lines (Emre *et al*. 2013). Black arrows on the fault traces indicate the relative motion of the faults. The fault ruptures of 2010 Mw6.1 Kovancılar; 2011 Mw5.4 Palu; 2020 Mw6.8 Sivrice earthquakes are shaded in pink, blue and red, respectively. Red stars represent the epicenters of the 2023, Kahramanmaraş earthquakes. AB: Amik Basin. SF: Sürgü Fault. KMTJ: Kahramanmaraş Triple junction. KOTJ: Karlıova Triple Junction. HF: Hatay Fault. AF: Amanos Fault. DSF: Dead Sea Fault. NAF: North Anatolian Fault. VFZ: Varto Fault Zone. YsF: Yesemek Fault. NF: Narlı Fault. YF: Yumurtalık Fault. T: Türkoğlu. TF: Toprakkale Fault. GB: Göksun Bend. DF: Possible continuation of the Doğanşehir Fault. Karasu Valley and Karlıova Basin (KB) are shown by striped areas. Dash black box shows the East Anatolian Fault Zone. Inset shows the locations of the historical earthquakes with M>7.0 (Duman and Emre, 2013; Nalbant et al. 2002; Kondorsskaya and Ulomow, 1999).

since with small magnitude seismicity (Güvercin et al., 2022). The 2020 Mw6.8 Sivrice earthquake, which ruptured ~45 km of the EAFZ from Palu to Pütürge was the largest on the EAFZ

during the instrumental period until the 2023 earthquakes (Konca et al., 2021). From the southwest of the Pütürge segment to the end of Amanos, the observations indicate low strain rate, low seismicity rate and long recurrence times of large historical earthquakes. Two largest magnitude earthquakes in 2023 occurred on a known seismic gap which did not experience similar large rupture since the historical earthquake of 1114 M>7 (Ambraseys, 1988, 2009). We present seismic activity before the seismic crisis, new observations from two largest events, rupture geometries and near-field ground displacements from sub-pixel correlation of satellite images, aftershock distributions and focal mechanism solutions, and a reevaluation of the seismic potential of the ruptured fault based on the large Mw7.8 earthquake on the EAF.

Data and Methods

We relocated three mainshocks and the aftershocks using the event database reported by Disaster and Emergency Management Authority (AFAD: https://tdvms.afad.gov.tr). The seismic waveform data from broadband and acceleration stations are used to revise and append the catalog to improve the locations of the aftershocks with Mw5.0+. The magnitudes reported by AFAD are used in the revised catalog. The completeness of the catalog provided by AFAD was high (M_c=3.8) and requires more detailed analysis to better characterize the seismic crisis. Here we only concentrate on the two largest events and big aftershocks during the first 2 weeks of the seismic activity. A new local velocity model with the station corrections was computed with the joint use of the aftershock data from the 2023 earthquakes and the catalog from the previous time period between 2012 and 2020 (See Güvercin et al., (2020) for the catalog and the computational details). The spatio-temporal evolution of the relocated seismicity is displayed in the Supplementary Material (Figure S1a) with the locations and uncertainties of the largest events (Figure S1b).

We used the focal mechanism solutions from the reports of various agencies (GCMT, GFZ, INGV, KOERI, AFAD, OCA, USGS) (Table S1) and obtained unreported mechanisms of M3.0+ events during the preseismic period from the regional waveforms using the Cut-and-Paste method (Table S2) (gCAP) (Zhao and Helmberger, 1994; Zhu and Helmberger, 1996; Zhu and Ben Zion, 2013). A total of 49 focal mechanism solutions are displayed in Figure 6, of which 9 of them are computed

here. The computational details for the relocation and the determination of source mechanisms are the same as Güvercin et al. (2022).

Coulomb stress analysis is performed for specified faults (Toda *et al.* 2011; Lin, J. and R.S. Stein, 2004) using the geometry of the EAFZ from Güvercin et al. (2022) while the receiver faults with no slip are adopted from the active fault map of the Turkish General Directorate of Mineral Research and Exploration (MTA) (Emre et al., 2023). The slip model for the Coulomb model the finite-fault model of USGS (2023), which is obtained from the teleseismic, and strong-motion and high-rate GNSS waveforms and GNSS static (https://earthquake.usgs.gov/earthquakes/eventpage/us6000jllz/finite-fault). We obtain the source-time functions of the two events by employing a preliminary finite fault model using teleseismic P and SH waves (Ji et al., 2002).

The 2D component of the surface deformation field is retrieved by correlation of pre and post event Sentinel-2 optical satellite images. The short time period between the two post-event images, which are both within 3 and 8 days of the earthquake sequence, means they likely contain relatively little post-seismic deformation, and any difference in displacement between the two images will be far below the threshold of the correlation technique (~1/10th pixel). We correlate band 8 of the Sentinel-2 scenes, which in this case gives the cleanest displacement fields, using the frequency-based correlator from the COSI-Corr software package (Leprince, et al., 2007). Additional details on the processing and denoising are presented in the Supplementary Material (Figure S2).

Seismic Activity Before the 2023 Ruptures

Figure 2 shows the seismicity evolution along the EAFZ from Jan 2012 to 06 Feb 2023 with magnitudes M2.5+. Overall, the seismicity rate is high from the Karlıova Triple Junction (KOTJ) to the western termination of the 2020 Mw6.8 Sivrice rupture. From the east of the Pütürge segment to the end of the Amanos, the seismicity rate is nearly uniform except for longitudes between 37.0-37.5 where the Karasu Valley elongates nearly in N-S direction and merges to the EAFZ (Figure 1,2). In this zone, a moderate size earthquake (Mw5.1) occurred on the Narlı Fault Zone in 2012. Other clusters towards the NE of Narlı Fault Zone and on the Pazarcık segment have been continuously active producing episodic seismic activities (Figure S1). Notable seismic

activity is observed, between 2012-2023, on the Yesemek Fault with earthquakes M3.0+, subparallel to the Amanos segment (Figure 2). The focal mechanism solutions of these earthquakes show dominant normal fault solutions with some left-lateral strike-slip component (Figure 2). An increase in the seismicity rate is observed within these clusters in 2022 (Figure 2a, yellow and gray shaded boxes, Figure 2b, yellow and gray shaded bars).

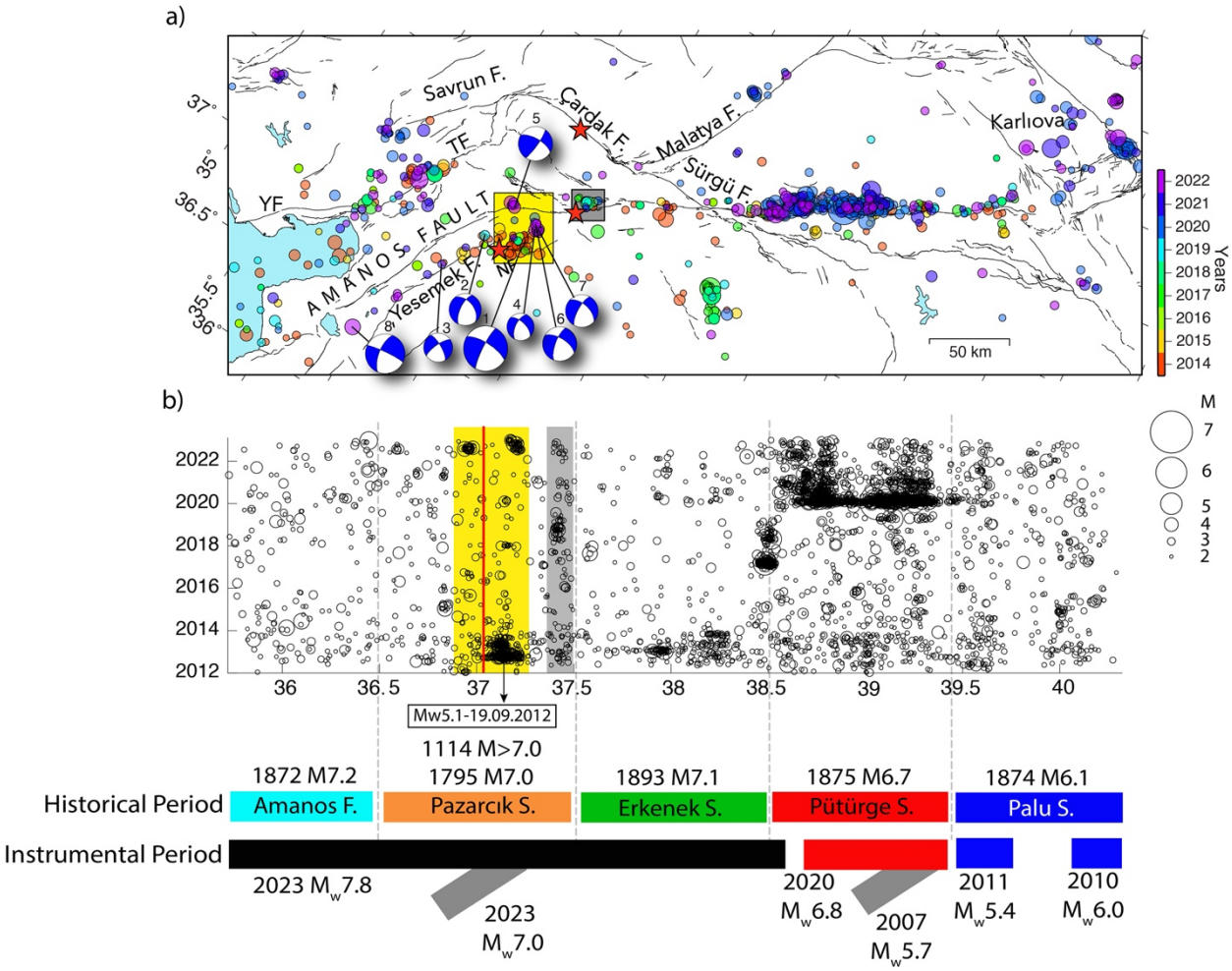

Figure 2: Time evolution of the seismic activity with M2.2+ on the EAFZ between Jan 2012-06 Feb 2023. a) The annual evolution of seismicity is displayed with colors and scaled with magnitudes. The blue beachballs represent the focal mechanisms of the earthquakes with M3.5+ before 2023 events (Table S2). ID number of each focal mechanisms is given near the beachballs. The segment names are adopted from Duman and Emre (2013). Yellow and gray boxes show the locations of long-term seismic clusters. Red stars indicate the epicenters of the 2023 earthquake sequence. b) Black circles represent the M2.2+ earthquakes scaled by magnitudes. The seismic activities in the yellow and gray boxes of the top figure are shown as shaded regions with the same colors on the time evolution. Red solid line marks the longitude of the 2023, M_w7.0, Narlı event.

The rupture lengths of the large earthquakes during the historical and instrumental periods are shown on the bottom with different colors.

Co-seismic Ruptures and Surface Offsets

Sub-pixel correlation of Sentinel-2 optical satellite images reveals the horizontal component of motion produced during the seismic sequence. The EW and NS components of the displacement field are consistent with left-lateral strike-slip motion (Figure 3a). The fault traces are clearly expressed as sharp discontinuities in the horizontal displacement field, which reveal a ~300 km and ~140 km surface rupture for the Mw7.8 and Mw7.6 earthquakes, respectively.

For the Mw7.8 earthquake highest surface slips are observed on the EAFZ between KMTJ and Sivrice segment between latitudes 37.5° and 38° with a peak value of 7 m (Fig. 3c). The rupture initiation along the Narlı fault, which corresponds to an Mw7.0 sub-event, is also observed as a change in the gradients on both components along a 30 km length (white box in Figure 3a, and Figure 4a,b). The surface offsets on the Narlı fault reveal significant normal component (Figure 4c,d), in accordance with the focal mechanism of the pre-seismicity in the vicinity (Figure 2).

In the east, a splay of ~10 km length trending east from the main rupture zone near the junction of Sürgü Fault, is observed (Figure 3a-b). When the rupture arrived near the Pütürge segment to the northeast, it deviated towards the east and terminated after propagating another 20 km. The optical correlation results show that the rupture stopped in the northeast, near the termination of the 2020 Mw6.8 Sivrice earthquake at Çelikhan, and at the Hatay graben at the southwestern end.

The rupture of the Mw7.6 event is also clearly expressed in the EW component, with decreasing magnitude to the east (Figure 3a). The surface rupture can be traced for a total of ~140 km, with left-lateral strike slip surface displacements of up to 8.5 m (Fig. 3d). The offset values decrease dramatically where the rupture zone orientation changes from E-W to SW-NE; slip values then rapidly taper for ~45 km between longitudes 37.5° and 38.0°. It is clear from the surface offsets that the rupture continued toward the NE, subparallel to the EAFZ, rather than continuing toward the Sürgü Fault in the east. At the western limit, the rupture continued towards the SW and ended

quite abruptly near Göksun. Both events show predominantly left-lateral displacements. Correlation bias, resulting from differencing reflectance conditions between the pre- and post-images (e.g. fresh snowfall in the post-image) adds a spatially correlated noise signal to the NS component, which currently limits our ability to resolve the fault-normal component of deformation (which is smaller in magnitude than the strike-slip component, and thus has a lower signal-to-noise ratio). Furthermore, we note that the left-lateral displacement estimates along the central section of the Mw 7.8 rupture may be slightly corrupted by the noisy NS component, given the NE-SW fault strike at this location (between 37.1° and 37.5°E).

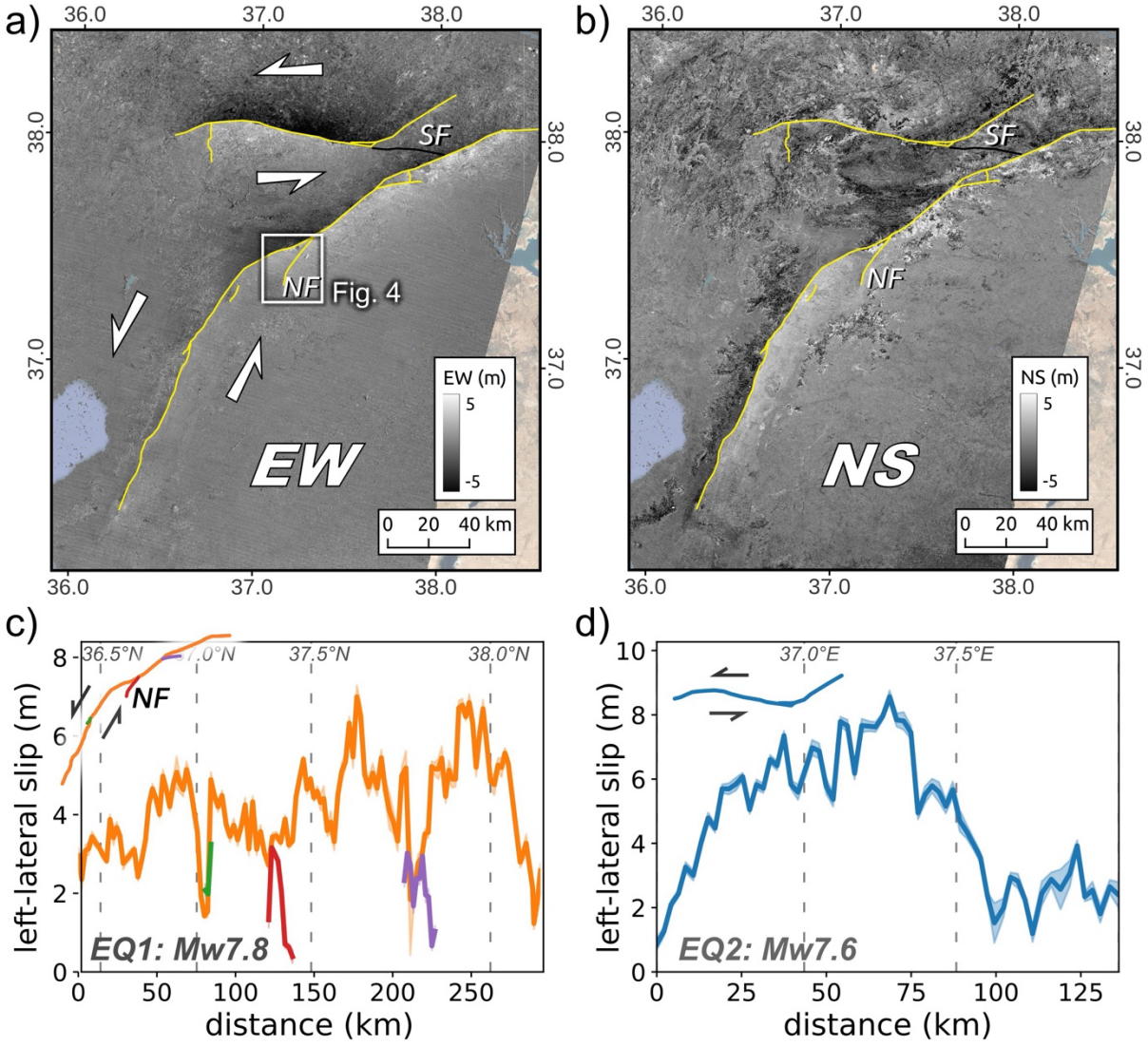

Figure 3: Image correlation maps showing (a) EW and (b) NS components of displacement from correlation of Sentinel-2 satellite images (see text for details). NF: Narlı Fault. SF: Sürgü Fault. White box shows the location of Figure 4. Yellow lines show the fault ruptures from both Mw7.8 and Mw 7.6 earthquakes. Along-strike left-lateral displacement profiles are shown for the (c) Mw7.8 (orange line), and (d) Mw7.6 (blue line) events. Various displacement profiles for ruptured sub-segments in (c) are also shown with different colours. Upper left insets in (c) and (d) show the rupture for each case in map view. Decreases in the localized slip generally correlate with geometric complexities.

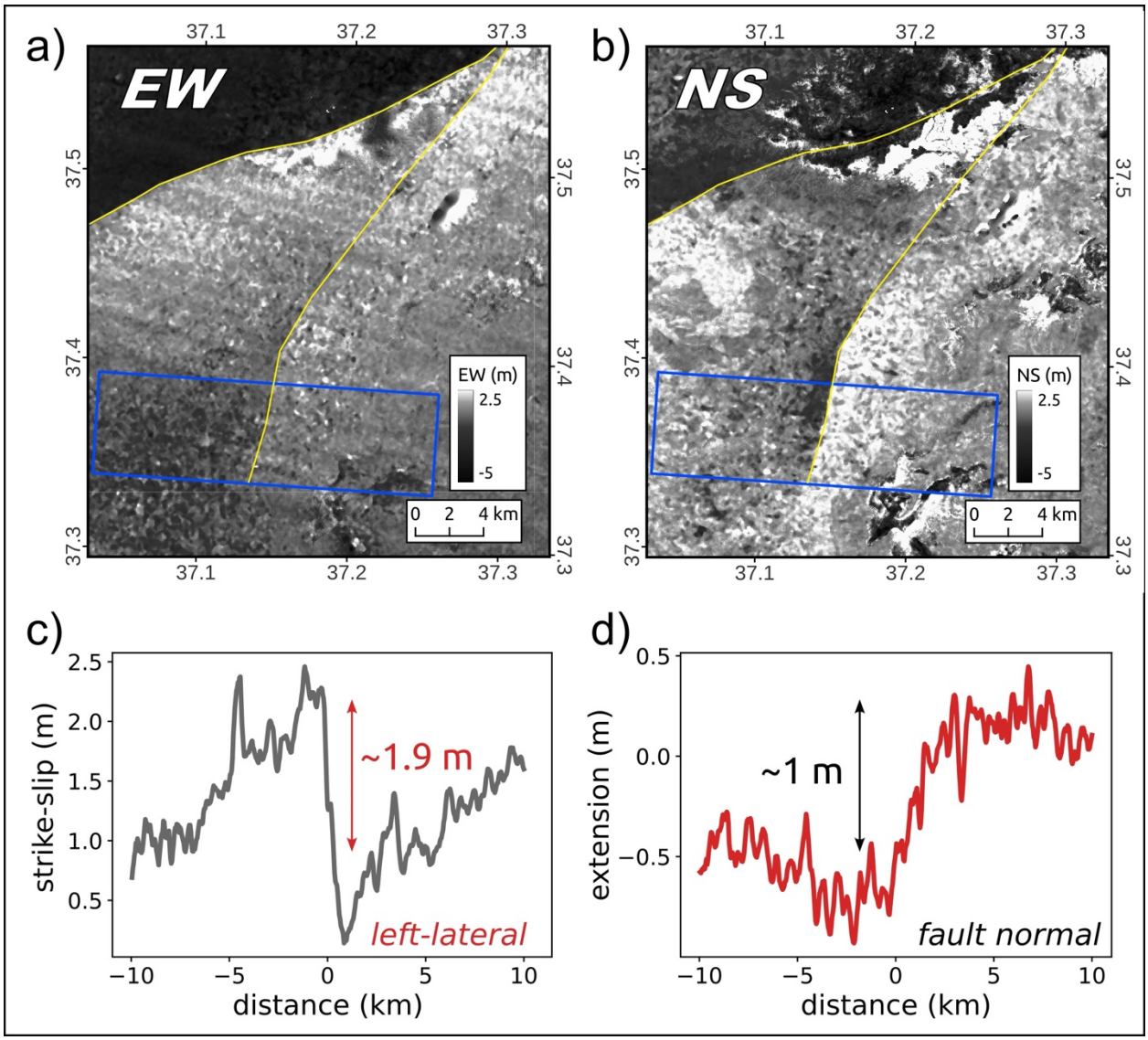

Figure 4: Image Correlation maps showing the (a) EW and (b) NS components of displacement for the region covering the Narlı Fault, which is the epicentral area of the ruptured Mw7.0 sub-event, which initiated slip on the larger Mw7.8 rupture. The color scale is modified to enhance the slip discontinuity on the Narlı Fault. Yellow lines highlight surface ruptures. Blue boxes show the

location of a stacked fault-perpendicular profile, from which we extract the left-lateral (c) and fault-normal (i.e. horizontal extension) components across the southern Narlı Fault rupture. Displacement on this structure featured left-lateral strike-slip with an extensional component, consistent with the focal mechanism solution.

Figure 5 shows the source time functions of the two mainshocks using teleseismic P and SH waveforms from a preliminary finite fault model in comparison to the several strike-slip earthquakes that occurred along the NAF and the EAFZ in the last 3 decades. The 1999 Mw7.4 İzmit and Mw7.1 Düzce earthquakes ruptured the northwest of the North Anatolian Fault with supershear rupture speeds and have very compact source time functions. The 2014 Gökçeada-Samothraki earthquake occurred along the North Aegean Trough with a very slow rupture velocity (~1.5 km/s) and generated an unusually long rupture length of ~90 km. The 2020 Sivrice earthquake ruptured ~45 km length of the adjacent northeast segment of the 2023 rupture without producing any surface offsets. The comparison shows that the first 20 s of the Mw7.8 event featured relatively moderate moment release rates, with a magnitude of ~7.0. This is consistent with the initial phase of the rupture with a relatively small ~Mw7.0 subevent which broke ~50 km long fault to the north before reaching to the EAFZ.

The accurate relocation of the Mw7.0 sub-event with horizontal uncertainties less than ~1km clearly shows that the rupture initiated on the subparallel Narlı fault not on the EAF (Figure S1b). The distance between the epicenter of the Mw7.0 sub-event and the EAF is about 20 km. The correlation of optical images also shows surface slip on the Narlı Fault where the hypocenter is located (Figure 4). These observations confirm that the Mw7.8 earthquake was the continuation of the Mw7.0 event initiated by the arrival of the rupture front to the EAFZ, ~20 s later (Fig. 4 and 5). The moment release increased significantly with a bilateral rupture propagation along the EAFZ. The complexity of the source time function is a consequence of the rupture of different segments along the EAFZ, while moment release in all the patches are quite significant with a total duration exceeding 80 s. The Mw7.6 Çardak earthquake on the other hand, has a duration of 40 s, and a very sharp onset consistent with the very high surface offsets observed in the epicenter area (Fig. 3-4).

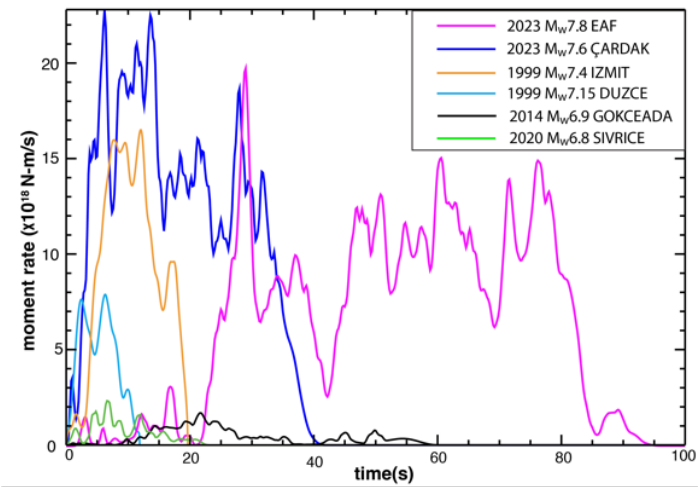

Figure 5: Comparison of source time functions for the 2013 Mw7.8 and Mw7.6 earthquakes along-side other recent strike-slip earthquakes on the NAF and the EAFZ. The source time functions of the 1999 Mw7.4 Izmit and Mw7.15 Düzce earthquakes are from the SCARDEC source time database (Vallee and Douet, 2016). The other source time functions are from finite-fault studies (Konca et al., 2018, Konca et al., 2021).

The Aftershock Distribution and Earthquake Source Mechanisms

Figure 6 shows the mainshocks and the aftershock distribution between 06th Feb 2023 and 20th Feb 2023. The colours are used to illustrate the time evolution of the aftershock activity. The early aftershocks clearly illuminate the rupture zone and are spatially consistent with the surface rupture obtained from image correlation (Figure S3 in Supplementary Material).

The location of the initial ~Mw7.0 subevent is precisely determined from the seismic stations in the near proximity of the epicentral region (Supplementary Material, Figure S1b). A small precursory event was also identified at several stations prior to the Mw7.0 event. The focal mechanism solution of the Mw7.0 subevent determined from the moment tensor inversion of the first 20 s of the near-field waveforms reveals a mechanism with a NE-SW left-lateral strike-slip motion with a normal component (Figure5, ID: 1a, Figure S4). It is worthwhile to mention the similarity of the source mechanisms of Mw7.0, 2023 and Mw5.1, 2012 (Figure 2, ID:1). The epicenters of both events hint that the same fault zone experienced ruptures of different lengths.

The Mw7.8 earthquake occurred ~20 s later with the arrival of the rupture front of the ~Mw7.0 subevent at the EAFZ, (the epicenter is marked as the intersection of the Mw7.0 rupture with the EAFZ). The largest aftershock with Mw6.6 occurred ~10 min later on the Amanos segment close to the epicenter of the Mw7.0 event.

The background seismicity was low during the interseismic period on the Çardak Fault (Figure 2). The only reported historical event on the Çardak Fault is the 1544, M6.8 earthquake (Kondorskaya and Ulomow, 1999). No notable pre-seismic activity is detected at the epicentral region of the Mw7.6 earthquake following the rupture of the Mw7.8 event. The most notable feature on the Mw7.6 rupture is the evolution of the seismic cluster at the western termination at the Göksun Bend having a continuation to the Savrun Fault. The aftershocks and the source mechanism solutions in this cluster show two distinct orientations nearly perpendicular to each other. The first cluster to the west of the rupture area has NE-SW orientations with strike slip geometry, consistent with the surface rupture of the Mw7.6 with the orientation of the Savrun fault (Figure 6, ID:3, 25, 30, 34). The second cluster nearly perpendicular to the first displays normal mechanism solutions (Figure 6, ID: 6, 14, 17, 39).

On 20 Feb 2023, 2 weeks after the Mw7.8 and Mw7.6 earthquakes, a third earthquake with Mw6.4 occurred on the Hatay fault, which bounds the city to the southeast. The aftershock activity was focused on the northwest of the mapped fault consistent with the source mechanism solutions (Figure 6, ID: 16-37), showing a NW-SE oriented normal fault (Figure 6, ID: 16-37). The offshore continuation of the activity in the İskenderun Bay is observed along the fault which extends to the Cyprus Arc in the Mediterranean Sea (Figure 1 and Figure 6). In the NE termination of the Mw7.8 rupture, the aftershock activity stops soon after the SW termination of 2020 Mw6.7 Sivrice rupture. These results suggest that the Mw7.8 rupture possibly stopped due to the change of the kinematics from strike-slip to normal, but then the stress loading due to this large earthquake was sufficient to rupture the Hatay Fault (Figure 7c inset, Figure S5).

Toward the northeast of the rupture area, a progressive increase of seismic activity within two weeks following the two large ruptures, extended to the Palu segment and finally reached to KOTJ in the northeastern continuation of the EAFZ. Two large earthquakes created a large zone of stress

perturbations far from the ruptured faults, triggering moderate size earthquakes of Mw5.0+ and clusters of seismicity (Figure 6). Two Mw5.0+ events in the Malatya and Bingöl are just few examples of distant triggering. The majority of these triggered events occurred within the previously observed long lasting seismic clusters (Karabulut et al., 2022) and are mostly associated with the geometric complexities such as bends and stepovers of the hosting faults, which are also prone to generate moderate size earthquakes. The absence of aftershocks between the eastern end of the Mw7.6 rupture at the Sürgü Fault and the EAFZ confirm the termination of coseismic rupture before reaching the EAFZ. However, the continuation of the seismicity to the northeast with a subparallel orientation to the Doğanşehir Fault (Figure 1) is well characterized by the lineament of the aftershocks and the focal mechanism solutions of Mw5.0+ earthquakes (Figure 6, ID: 4, 24, 26, 28, 36).

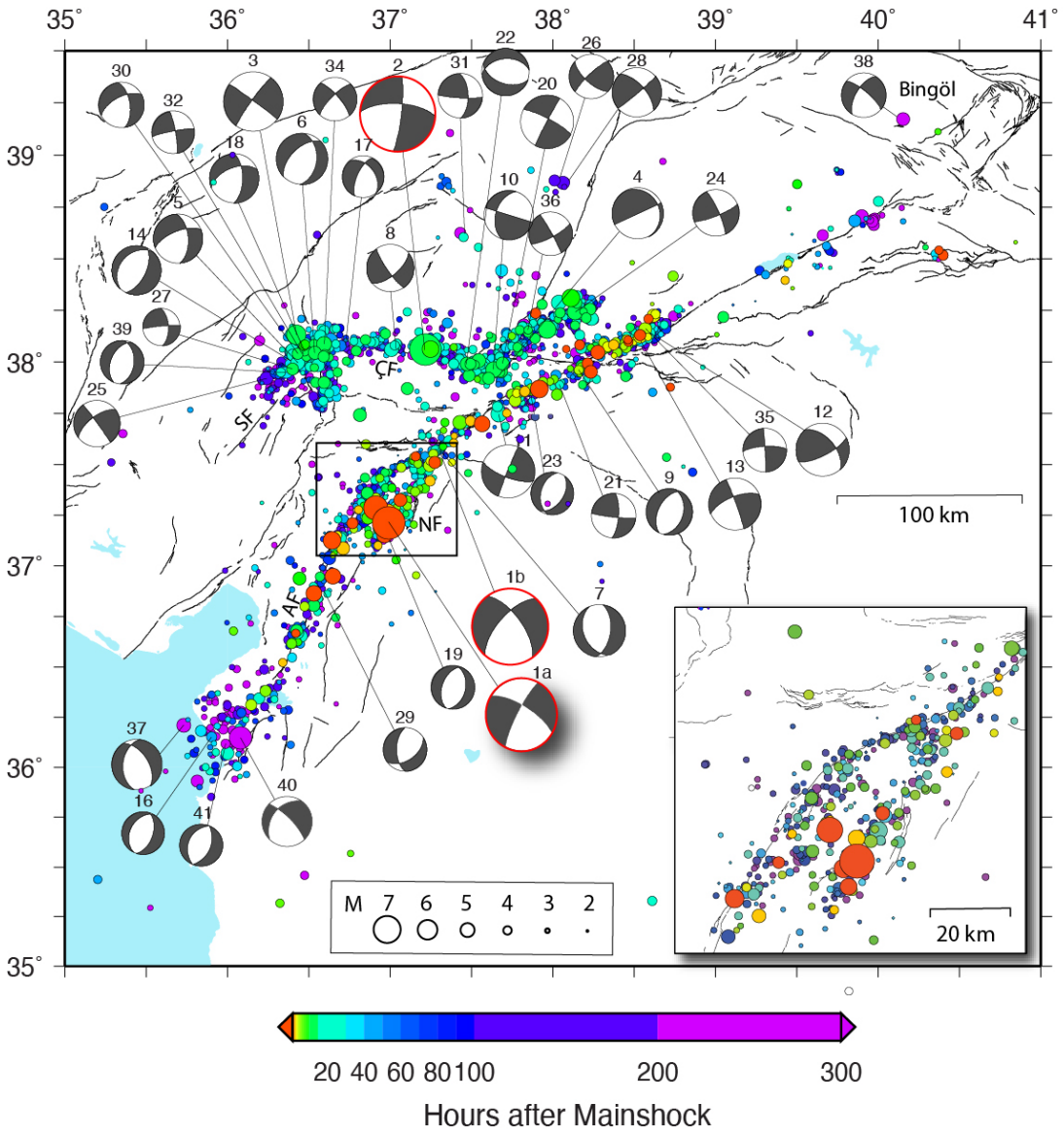

Figure 6: Map view of the aftershock locations during the first 15 days of seismic activity between February 6th and 21th. The colours show the time evolution of the aftershocks scaled by magnitudes. The beachballs show the source mechanism solutions of the aftershocks with the numbers on the top and listed in Table S1. The inset figure shows the zoom of the seismic activity (black square) in the epicentral region of the Mw7.0 earthquake.

Coulomb Stress Analysis

To illustrate the interactions between the two largest earthquakes, and how these large earthquakes may control the distribution of the aftershocks at the terminations of two ruptures, as well as the neighboring faults, we modelled the changes in Coulomb failure stress.

Figure 7a shows the Coulomb stress changes on receiver faults following the Mw7.8 earthquake. The stress increase is observed at the future epicenter of the Mw7.6 earthquake on the Çardak Fault by ~1.0bar. The southern termination of the rupture experiences a stress increase along the DSF and the Hatay fault which ruptured with a Mw6.4 earthquake two weeks later. Figure S5 shows the Coulomb stress change (~1bar) on the Hatay Fault which was built as a receiver fault with the mechanism of the Mw6.4 event (Table S1). The NE continuation of the EAFZ also experienced an increase in Coulomb stress along the Pütürge and Palu segments.

Figure 7b shows the distribution of the aftershocks during the first 9 hours before the Mw7.6 event with the Coulomb stress changes calculated at a depth of 10 km using the geometry of the Çardak Fault as specified faults. The distribution of the early aftershocks is consistent with the areas of Coulomb stress increases.

Figure 7c illustrates the Coulomb stress analysis following the ruptures of Mw7.6 and Mw7.8 earthquakes. The cumulative stress transfer of both ruptures observed on the Sivrice and Palu segments reaches to ~1 bar. The Malatya fault experienced stress increase up to ~1.5 bar due to the Mw7.6 Çardak earthquake.

Figure 7d shows the distribution of the aftershocks during the first 2 weeks after the 6th February, and the cumulative Coulomb stress change at 10 km depth using the geometry of the EAFZ as specified faults. The distribution of the aftershocks is well correlated with the cumulative Coulomb stress increase, especially along the northern segments of EAFZ and Malatya fault (Figure 7d). A large increase in Coulomb stress (~1.5 bars) is observed at the western termination of the ÇF with a highly active zone of aftershock seismicity.

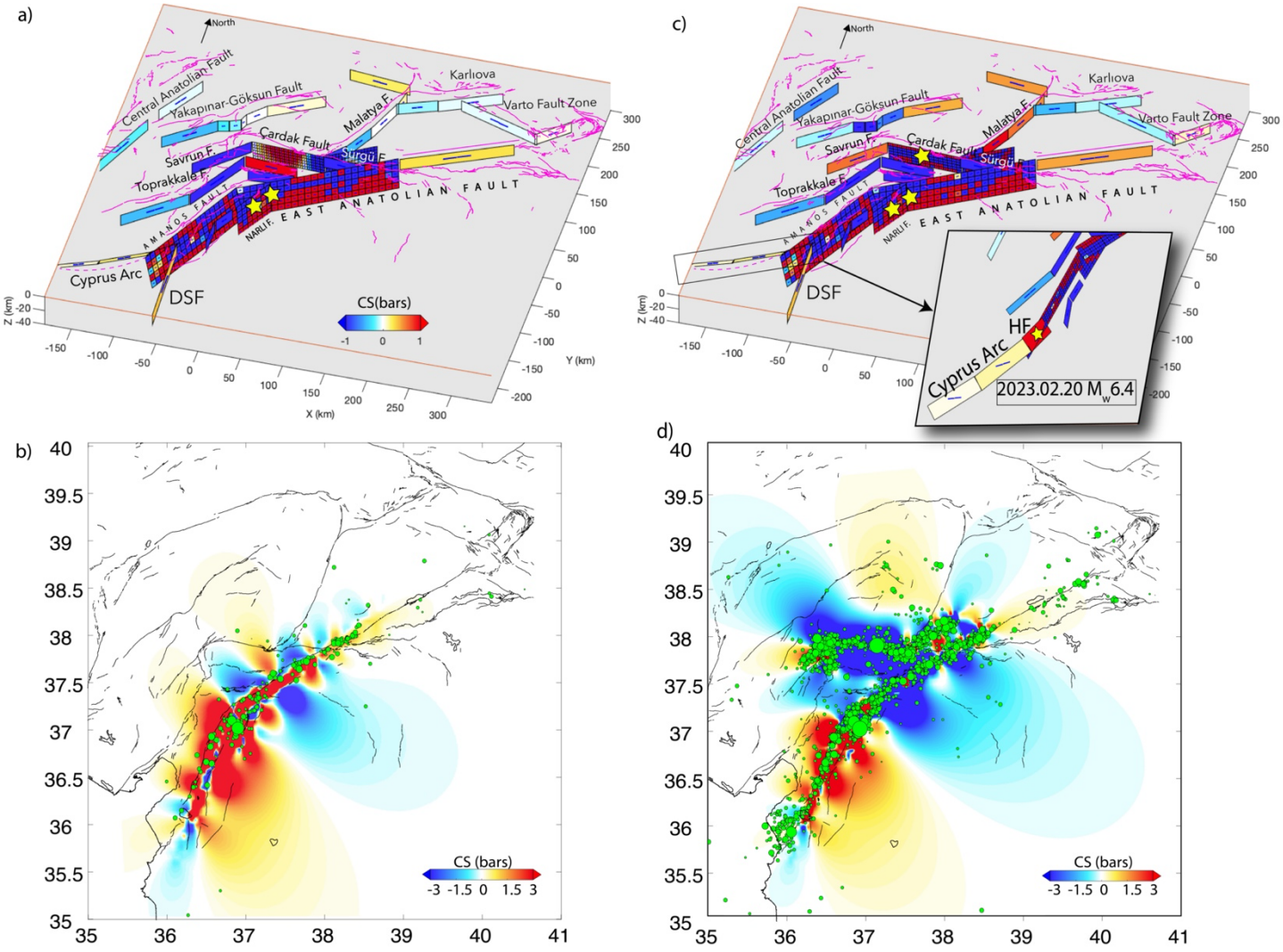

Figure 7: Coulomb stress analysis due to 2023 earthquake sequences. a) Coulomb stress changes on receiver faults following the Mw7.8 earthquake. Yellow stars show the locations of the Mw7.0 and Mw7.8 events. b) Coulomb stress changes at 10 km depth after the Mw7.8 earthquake calculated using specified faults with average geometry of the Çardak Fault. Green circles represent the epicenters of the aftershocks during first 9 hours before the Mw7.6 Çardak earthquake. c) Cumulative Coulomb stress changes on receiver faults after two large earthquakes. Inset: Stress changes on the Hatay Fault and Cyprus Arc. Yellow star represents the 20 Feb. 2023 Mw6.4 Hatay earthquake. d) Cumulative Coulomb stress changes at 10 km depth after two large earthquakes calculated using specified faults with average geometry of the EAFZ. Green circles show the epicenters of the aftershocks during the first 15 days of the activity and scaled by magnitude. Faults are shown by pink and black lines (Emre et al., 2013).

Discussion

The initiation and triggering of two large earthquakes and the rapid growth of the aftershock zone together with the increased level of pre-seismic activity are indications that the ruptured segments of the EAFZ were at a state of critical stress. The stress on the fault within a low strain rate environment may stay long near failure during the late stages of interseismic period. The rupture would start at any location on the fault that is in a critical state, and thus sensitive to stress perturbations. The epicenter of the Mw7.8 earthquake was far from the southwestern termination of the 2020 Mw6.9 Sivrice earthquake where the Coulomb stress increased, but instead occurred at a splay fault in Narlı, where high seismic activity rate within a seismic cluster is observed with some temporal accelerations. The focal mechanism solutions of the earthquakes in this cluster show dominant normal faulting with largest, 2012 Mw5.1 event. The surface offsets on this segment also shows significant extension. Therefore, we conclude that the earthquake initiated within a zone of continuous seismic activity with the occurrence of Mw5.1 earthquake in 2012 and progressively weakened resulting in the rupture of the Mw7.0 subevent. Similar observations were made for the Mw7.4 1999 Izmit earthquake (Bouchon et al., 2022).

1. Did a Permanent Barrier Stop the 2020 Sivrice and 2023 Kahramanmaras Earthquakes?

The termination of the 2023 Mw7.8 earthquake in the east and the termination of the 2020 Mw6.8 Sivrice earthquake in the west share a similar zone where several faults converge to the EAFZ. Correlation of optical images before and after the earthquake also reveals that the Mw7.8 event deviated from the main fault plane and terminated by rupturing a fault to the east.

The Sürgü fault, situated to the west of this junction, did not break in either of the two large earthquakes of 2023. The Mw7.6 earthquake started toward on the Çardak fault, which is to the west of the Sürgü fault, but could not penetrate through the Sürgü fault, instead deviating to the northeast. Despite being mapped as an active fault (Emre et al., 2013) and previously reported as seismically active (e.g., Güvercin et al., 2022), a clear gap is apparent in the aftershock activities of the Mw7.8 rupture and the continuation of the Mw7.6 event along the Sürgü Fault. The Coulomb stress analysis shows that the Mw7.8 event loaded the Çardak Fault, but led to a stress decrease

along the Sürgü fault. The lack of slip or the aftershocks along the Sürgü fault may be related to the stress shadow induced by the Mw7.8 event.

The distribution of seismicity with respect to the ruptures indicates that the dip direction of the EAF may also change around this junction. The detailed study of the aftershock activity of the Sivrice earthquake indicates a northwest dipping fault (Güvercin et al, 2022). The aftershocks of the Mw7.8 earthquake are located along the southwest of the surface fault trace indicating a southwest dip in accordance with the focal mechanisms in this zone. Thus, we conclude that the change in the fault dip may also had an influence of the rupture termination.

These observations imply that the zone where Sürgü, the EAFZ and the faults related to the Bitlis Suture to the east comprise a persistent barrier to the ruptures in both directions. The rupture termination of the 2020 Mw6.8 Sivrice and the 2023 Mw7.8 earthquakes may reflect the impact of this boundary, which led to the clamping of the nearby Sürgü fault.

2. Synchronization of two largest earthquakes

The geodetic and geologic slip rates of the Cardak Fault are estimated between 1.5-2.5 mm/yr, much lower than the rates for the Amanos Fault (~4.6 mm/yr) and the East Anatolian Fault (~6.8 mm/yr) (Reilinger et al. 2006; Duman and Emre, 2013; Koç and Kaymakçı, 2013). Furthermore, the historical earthquakes on this fault are not well known. It is anticipated that the recurrence time for an earthquake as large as Mw7.6 on the Çardak Fault is much longer than those on the EAF. The synchronization of two largest 2023 earthquakes (~9 hours apart) implies significant time advance of the Mw7.6 rupture due to the loading or the unclamping of the Çardak Fault as a result of the Mw7.8 rupture. The Coulomb stress increase due to the Mw7.8 rupture with a significant change in the orientation of the NE striking EAF and NNE striking Amanos faults around KMTJ may have further facilitated the rupture of the Çardak Fault. The cumulative motion of the two faults together is consistent with the counterclockwise motion of Anatolia.

3. The stress perturbations and seismic activation at regional scale

The two largest earthquakes of 2023 ruptured more than 500 km of the EAFZ. A large aftershock zone and its progressive expansion to surroundings imply the region is susceptible to the activation of swarm type seismicity and moderate size earthquakes. The loading of the fault at various scales during the post-seismic period and the relaxation of the lower crust will load the fault far from the ruptured faults. Many of the faults, e.g., Malatya, Tuz Gölü, Ecemiş, display low strain rates and long recurrence times. Therefore, it is not predictable how loading will influence timing of the rupture on these faults. In the meantime, the activity following the East Anatolian Doublets on these faults with Mw5.0+ indicate these faults may have been loading (e.g., Mw5.1 Malatya, Mw5.1 Erciyes, Mw5.3 Konya) (Figure S6). On the western termination of the Mw7.6 rupture at Göksun Bend, the aftershock activity follows the orientation of the Savrun Fault, with NE-SW trend towards the Adana Basin. In the Adana Basin, the seismicity is diffuse, normal and strike slip faulting are related to the Missis-Kyrenia Fault zone on the north of Cyprus.

4. 2013 Earthquake Cycle, Moment Deficit and Inferences on Seismic Hazard Assessment

In order to assess the seismic hazard in a region, it is crucial to combine information on the historical earthquakes, paleoseismic studies, geodetic measurements of crustal deformation and instrumental earthquake observations. We attempt to assess the seismic potential of this large event on the EAFZ by considering geodetic slip rates and the Gutenberg-Richter (GR) parameters. This approach follows Stevens and Avouac (2021) and was applied to the EAFZ for each segment separately by Güvercin et al., (2022) where the seismic strain accumulation around the fault is equated to the moment release by earthquakes following the GR law. The updated approach yields both the maximum expected magnitude (Mmax) (1) and a return period (Tr) (2) by extending the whole ruptured section of the EAFZ in light of the recent earthquake.

$$M_{max} = \frac{1}{3/2 - b}\left(log_{10}\left(1 - \frac{2b}{3}\right) + log_{10}(\alpha . \dot{m}) - 9 - a\right) \quad (1)$$

where α is a constant related to the interseismic coupling and $\dot{m}$ is the moment build-up rate.

$$T_r = 1/10^{(a-bM_{max})} \quad (2)$$

Table 1 shows the parameters used in the analysis. The geodetic slip-rates on the ruptured faults are ~1-3 mm/yr along the southwest end and increases to ~10 mm/yr to the northeast. (The details of the method used here is given in the Supplementary Materials.)

Here, we consider several scenarios. The earthquake in 1114 is considered as a large event (M7.8) with similar extent to the 2023 earthquake (Ambraseys 1988). In the explored scenarios, we aim to better define the seismic cycle of the EAF. Considering the earthquakes of February 6th, 2023 represent the end of the earthquake cycle on the EAFZ, the calculated cumulative moment build-up is expected to be equal to the cumulative moment release.

Figure 8 compares the cumulative geodetic moment build-up (CMB) and the cumulative seismic moment release (CMR) for three scenarios based on historical earthquakes. In the first scenario (S1), we take all the large historical events as reported (Duman and Emre, 2013; Ambraseys, 1988), considering moment build up since the 1114 (M7.8) earthquake, and the moment releases of 1893 (M7.0); 1795 (M7.2) and 1782 (M7.1) events (Table 2). In the second scenario (S2) we assume that the accumulated moment has been completely released in the last event cycle by the 1893 (M7.0); 1795 (M7.2) and 1782 (M7.1) events. The corresponding Gutenberg-Richter parameters are given in Figure 8a. In both scenarios, the CMR is one order of magnitude greater than the CMB.

Based on these two scenarios, we developed a third scenario (S3), in which we adjusted the magnitudes of the historical earthquakes to catch up the accumulated moment. The corresponding GR parameters are given in Figure 8a, while Figure 8b shows the cumulative moment release calculated for S1, S2 and S3 with accumulated cumulative geodetic moment built-up. The *a-value* represents the total seismicity rate of the region while the b-value is used to describe the frequency of the earthquake size distribution. The b values for S1, S2 and S3 are similar (~1) while the a values are 4.6, 4.9, and 5.1 for S1, S2 and S3 respectively.

Even if we consider the cumulative build up since the great 1114 event, the suggested magnitudes of the 18th and 19th century earthquakes still release significant moment leading to insufficient moment accumulation. The results indicate that the magnitudes of these historical earthquakes are likely to be overestimated by ~0.4 or some of them may not have actually ruptured the EAFZ. The analysis of Mmax and Tr show that the uncertainties in the magnitudes of the historical earthquakes bias the estimates in terms of length and time. Therefore, the last reported historical earthquakes cannot be representative of a complete earthquake cycle. The observations are not sufficient for the Çardak Fault to perform similar analysis to determine Mmax and Tr.

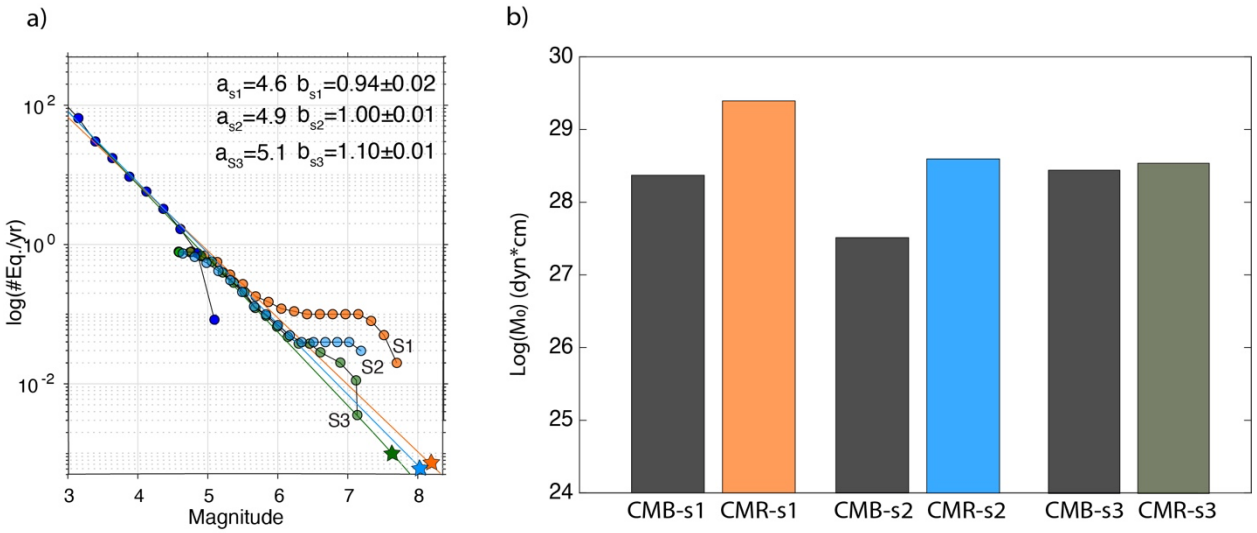

Figure 8: The seismic potential of the EAFZ estimated from geodetic strain rates. a) The Gutenberg-Richter relationship computed for rupture area of the 2023 earthquakes. The orange, light blue and green circles represent the long-term catalogs in S1, S2 and S3 respectively. Dark blue circles represent the short-term catalog between 2007-2022. The orange, light blue and green solid lines represent the GR fits of the merged catalog with historical events for S1, S2 and S3, respectively. The a and b values of the GR are shown at the upper right corner. b) The comparison of the cumulative moment build-up (CMB) and the cumulative moment release (CMR) for three different scenarios.

Table 1: Geodetic and seismologic parameters on the 2023 events along DAF. NOE: Number of events. Geodetic strain accumulation rates are from Reilinger et al., (2006). The second row with * is obtained from the rate of the earthquakes with M_c=2.5 per year between 2007-2019 (Güvercin et al., 2022).

	ERKENEK Segment	**PAZARCIK Segment**	**AMANOS Fault**
b-value (2007-2019)	1.30	1.10	1.10
*b-value (Since ~largest reported eq.)	0.88	0.94	0.92
α	0.5	0.5	0.5
Seismic Slip Rate (mm/yr) (2007-2019)	<1	<1	<1
Geodetic strain accumulation rates (mm/yr) (2007-2019)	6.5	4	3
Dip Angle	80	80	80
M of Largest Eq. recorded (2007-2019)	5.7	4.7	5.0
M of Largest Eq. recorded (2023 aftershocks)	5.3	5.3	5.7

Table 2: Seismic potential of the EAFZ for 3 scenarios using geodetic strain rates from Weiss et al. (2020).

	Scenario 1 (1114)	Scenario 2 (1114-1893-1795-1782)	Scenario 3 (1114-1893-1795-1782)
M	7.8	7.7-7.1-7.2-7.0	7.1-6.4-6.5-6.3
Mmax	7.8-8.0	7.9-8.1	7.8-7.9
Tr	1300-2000	1600-2500	700-1000

Conclusions

The 2023 earthquakes are an important reminder that moment accumulation since the previous large earthquake, and simple assumptions of earthquake recurrence rates are too simplistic to understand the extreme events. A section of a fault zone that releases moment partially in one seismic cycle, can break with much larger moment in the next cycle depending on the stress conditions along neighboring sections of the fault (Konca et al., 2008, Kaneko et al., 2010). The surface rupture and the moment rate function of the 2023 Mw7.8 earthquake shows that this event ruptured multiple segments, and that stress on the fault was high for a significant portion of the EAFZ. The rupture was stopped at a clear barrier in the northeast where three faults connect together and the fault dip direction along the EAFZ changes.

The Mw7.8 earthquake initiated along a subparallel fault where significant long term seismic activity was observed before the mainshock, indicating that the rupture initiated at a location within a zone weakened prior to the rupture. The rupture of the Mw7.6 event 9 hours later significantly reflects the stress changes induced by the previous Mw7.8 mainshock.

The combination of the two events led to a stress increase on several large fault zones in the surrounding region including the eastern Cyprus arc, the Dead Sea Fault and several faults in the east Anatolia. However, two largest 2023 events changed the state of stress of the entire Anatolian plate, with significant internal deformation. Considering that the seismic activity following these two earthquakes extends to further than ~300 km away from the rupture zone, it is possible that the faults in the entire Anatolian plate are prone to generate high level seismic activity and moderate size earthquake for decades during the postseismic and the relaxation of the lower crust.

Acknowledgments

We would like to thank to the Disaster and Emergency Management Authority (AFAD) for making available the seismic waveform data and the earthquake catalogs extensively used in this study (https://tdvms.afad.gov.tr/). The waveform data are also used from the seismic stations operated by Bogazici University, Kandilli Observatory and Earthquake Research Institute, Regional Earthquake-Tsunami Monitoring Center (https://doi.org/10.7914/SN/KO). We would like to thank to Professor James Jackson, an anonymous reviewer and the editor, Dr. Yıldırım Dilek, for their comments which significantly improved the manuscript. We benefitted from the discussions with Esen Arpat, Celal Şengör and Professor Dan McKenzie during his visit at Kandilli Observatory.

References

AFAD (Disaster and Emergency Management Presidency), 1990. National Seismic Network of Turkey (DDA). International Federation of Digital Seismograph Networks. http://tdvm.afad.gov.tr/.

Aktuğ, B., Özener, H., Doğru, A., Sabuncu, A., Turgut, B., Halıcıoğlu, K., Yılmaz, O., 2016. Slip rates and seismic potential on the East Anatolian Fault System using an improved GPS velocity field, J. Geodyn., 94-95, 1–12.

Ambraseys, N.N., 1989. Temporary seismic quiescence: SE Turkey, Geophys. J. Int., 96, 311–331.

Ambraseys, N. N., 2009 "Earthquakes in the Mediterranean and Middle East: A Multidisciplinary Study of Seismicity upt o 1900" Cambridge University Press.Arpat, E., Şaroğlu, F. ,1972. The East Anatolian Fault System; Thoughts on its Development. *Bull. Miner. Res. Explor.*, 78

Barka, A.A. & Kadinsky-Cade, K., 1988. Strike-slip fault geometry in Turkey and its influence on earthquake activity, Tectonics, 7, 663–684.

Bayrak, E., Yılmaz, S., Softa, M., Turker, T. & Bayrak, Y., 2015. Earthquake hazard analysis for East Anatolian Fault Zone, Turkey, Nat. Hazards, 76, 1063–1077

Bouchon, M., Socquet, A., Marsan, D., Guillot, S., Durand, V., Gardonio, B., Campillo, M., Perfettini, H., Schmittbuhl, J., Renard, F., Boullier, A-M., 2022., Observation of rapid long-range seismic bursts in the Japan Trench subduction leading to the nucleation of the Tohoku earthquake, Earth and Planetary Science Letters, Volume 594,2022, 117696, ISSN 0012-821X.

Dewey, J.F., Pitman, W.C., Ryan, W.B.F. & Bonnin, J., 1973. Plate tectonics and the evolution of the Alpine system, Bull. geol. Soc. Am., 84(10), 3137–3180.

Duman, T.Y. & Emre, O., 2013. The East Anatolian Fault: geometry, segmentation and jog characteristics, Geol. Soc. Spec. Publ., 372, 495–529.

Emre, Ö., Duman, T.Y., Ozalp, S., Elmacı, H., Olgun, S. & Saroğlu, F., 2013. Active Fault Map of Turkey with an Explanatory Text 1:1,250,000 Scale. Special Publication Series. 30. General Directorate of Mineral Research and Exploration.

GCMT, 2023. https://www.globalcmt.org

GFZ, 2023. https://geofon.gfz-potsdam.de

Gülerce, Z., Shah, S.T., Menekşe, A., Özacar, A.A., Kaymakci, N., Çetin, K.O., 2017. Probabilistic seismic-hazard assessment for East Anatolian Fault zone using planar fault source models, Bull. seism. Soc. Am., 107, 2353–2366.

Güvercin SE, Karabulut H, Konca AÖ, Doğan U, Ergintav S., 2022. Active Seismotectonics of the East Anatolian Fault. Geophys. J. Int. (2022) 230, 50–69. https://doi.org/10.1093/gji/ggac045.

Hempton, M.R., Dewey, J.F. & Sarog ˘lu, F., 1981. The East Anatolian trans- form fault: along strike variations in geometry and behavior, EOS, Trans. Am. geophys. Un., 62, 393.

Herece, E., 2008. Doğu Anadolu Fayı (DAF) Atlası, general directorate of mineral research and exploration, Spec. Publ. Ankara, Ser. Number, 13.

INGV, 2023. http://autorcmt.bo.ingv.it/quicks.html

Jackson, J. & McKenzie, D., 1984. Active tectonics of the Alpine–Himalayan Belt between western Turkey and Pakistan, Geophys. J. R. astr. Soc., 77, 185–264.

Ji, C., Wald, D. & Helmberger, D., 2002. Source description of the 1999Hector Mine, California Earthquake, Part I: wavelet domain inversiontheory and resolution analysis, Bull. seism. Soc. Am., 92(4), 1192–1207.

Leprince, S., S. Barbot, F. Ayoub, and J. P. Avouac, 2007. Automatic, precise, ortho-rectification and co-registration for satellite image correlation, application to seismotectonics, IEEE Trans. Geosci. Rem. Sens. 45, no. 6, 1529–1558.

Kaneko, Y., Avouac, JP. & Lapusta, N., 2010. Towards inferring earthquake patterns from geodetic observations of interseismic coupling. Nature Geosci 3, 363–369, https://doi.org/10.1038/ngeo843.

Karabulut, H, Bouchon, M., Schmittbuhl, J., 2022. Synchronization of small-scale seismic clusters reveals large-scale plate deformation, Earth Planets Space 74, 158 (2022). https://doi.org/10.1186/s40623-022-01725-z.

Koç, A. & Kaymakci, N., 2013. Kinematics of Sürgü Fault Zone (Malatya, Turkey): a remote sensing study, J. Geodyn., 65, 292–307.

KOERI, 2023. http://www.koeri.boun.edu.tr/sismo/2/moment-tensor-solutions/.

Konca, A. O., Avouac, J.-P., Sladen, A., Meltzner, A. J., Sieh, K., Fang, P., et al., 2008. Partial rupture of a locked patch of the Sumatra megathrust during the 2007 earthquake sequence. Nature, 456, 631–635. https://doi.org/10.1038/nature07572.

Konca, A. O., Cetin, S., Karabulut, H., Reilinger, R., Dogan, U., Ergintav, S., et al., 2018. The 2014, MW6.9 North Aegean earthquake: Seismic and geodetic evidence for coseismic slip on persistent asperities. Geophysical Journal International, 213(2), 1113–1120. https:// doi.org/10.1093/gji/ggy049.

Konca, A.Ö. Karabulut, H., Güvercin, S.E., Eskiköy, F., Özarpacı, S., Özdemir, A., Floyd, M., Ergintav, S., Doğan, U., 2021. From interseismic deformation with near-repeating earthquakes to co-seismic rupture: a unified view of the 2020 Mw6.8 Sivrice (Elazığ) Eastern Turkey Earthquake, Journal of Geophysical. Research., 126-10, e2021JB021830.

Kondorskaya, N. V., Ulomov, V. I., 1999. Special catalogue of earthquakes of the Northern Eurasia (SECNE). http://www.seismo.ethz.ch/static/gshap/ neurasia/ nordasiacat.txt, 3 May, 2015.

Lin, J. and R.S. Stein, 2004. Stress triggering in thrust and subduction earthquakes, and stress interaction between the southern San Andreas and nearby thrust and strike-slip faults, Journal of Geophysical Research, v. 109, B02303, doi:10.1029/2003JB002607.

Mahmoud, Y. et al., 2013. Kinematic study at the junction of the East Ana- tolian Fault and the dead sea fault from GPS measurements, J. Geodyn., 67, 30–39.

McKenzie, D., 1972. Active tectonics of the Mediterranean region, Geophys. J. Int., 30, 109–185.

Muehlberger, W.R. & Gordon, M.B., 1987. Observations on the complexity of the East Anatolian Fault, Turkey, J. Struct. Geol., 9, 899–903.

OCA, https://sismoazur.oca.eu/#/ focal_mechanism/emsc/.

Şaroğlu, F., 1985. Doğu Anadolu'nun neotektonik donemde jeolojik ve yapısal evrimi: Istanbul Universitesi, PhD thesis, Fen Bilimleri Enstitüsü.

Şengör, A.M.C., 1979. Mid-Mesozoic closure of Permo-Triassic Tethys and its implications, Nature, 279, 590–593.

Stevens, V. L. & Avouac, J. P., 2021. On the relationship between strain rate and seismicity in the India-Asia collision zone: implications for proba- bilistic seismic hazard, Geophys. J. Int., 226, 220–245.

Tan, O., Pabuççu, Z., Tapırdamaz, C. M., İnan S., Ergintav S., Eyidoğan, H., Aksoy, E., Kuluöztürk, F., 2011. Aftershock study and seismotectonic implications of the 8 March 2010 Kovancılar (Elazığ, Turkey) earthquake (MW = 6.1), Geophys. Res. Lett., 38, 4–9.

Toda, S., R. S. Stein, K. Richards-Dinger and S. Bozkurt, 2005, Forecasting the evolution of seismicity in southern California: Animations built on earthquake stress transfer, Journal of Geophysical Research, v. 110, B05S16, doi:10.1029/2004JB003415.

USGS (2023), https://earthquake.usgs.gov/earthquakes/eventpage/us6000jllz/finite-fault.

Vallee, M., & Douet, V., 2016. A new database of source time functions (STFs) extracted from the SCARDEC method. Physics of the Earth and Planetary Interiors, 257, 149–157. https://doi.org/10.1016/j.pepi.2016.05.012

Yönlü O., Altunel, E. & Karabacak, V., 2017. Geological and geomorphological evidence for the southwestern extension of the East Anatolian Fault Zone, Turkey, Earth planet. Sci. Lett., 469, 1–14

Zhao, L.-S. & Helmberger, D. V., 1994. Source estimation from broadband regional seismograms, Bull. seism. Soc. Am., 84, 91–104.

Zhu, L. & Ben-Zion, Y., 2013. Parametrization of general seismic po- tency and moment tensors for source inversion of seismic waveform data, Geophys. J. Int., 194, 839–843.

Zhu, L. & Helmberger, D. V., 1996. Advancement in source estimation techniques using broadband regional seismograms, Bull. seism. Soc. Am., 86, 1634–1641.